Arch Appl Mech (2007) 77: 339–351
DOI 10.1007/s00419-007-0112-6

ORIGINAL

Hiroshi Yabuno · Koji Tsumoto

Experimental investigation of a buckled beam under high-frequency excitation

Received: 3 February 2006 / Accepted: 1 December 2006 / Published online: 14 February 2007

Abstract In this paper, we investigate theoretically and experimentally dynamics of a buckled beam under high-frequency excitation. It is theoretically predicted from linear analysis that the high-frequency excitation shifts the pitchfork bifurcation point and increases the buckling force. The shifting amount increases as the excitation amplitude or frequency increases. Namely, under the compressive force exceeding the buckling one, high-frequency excitation can stabilize the beam to the straight position. Some experiments are performed to investigate effects of the high-frequency excitation on the buckled beam. The dependency of the buckling force on the amounts of excitation amplitude and frequency is compared with theoretical results. The transient state is observed in which the beam is recovered from the buckled position to the straight position due to the excitation. Furthermore, the bifurcation diagrams are measured in the cases with and without high-frequency excitation. It is experimentally clarified that the high-frequency excitation changes the nonlinear property of the bifurcation from supercritical pitchfork bifurcation to subcritical pitchfork bifurcation and then the stable steady state of the beam exhibits hysteresis as the compressive force is reversed.

Keywords High frequency · Buckling · Bifurcation · Dynamic stabilization

1 Introduction

Interest of the usage of high-frequency excitation has focused on changing the linear and nonlinear dynamics of mechanical systems (a comprehensive survey on the application of high-frequency excitation is found in [1,2]). For example, it has been known for a long time that a pendulum can be stabilized in the inverted position by high-frequency excitation [3,4]. Also, a bifurcation control method under high-frequency excitation is proposed for the motion control of an underactuated manipulator without state feedback [5]. As seen from this study, the high-frequency excitation can cause the perturbation of the bifurcation and can modify not only linear, but also nonlinear properties inherently existing in systems.

In the present study, we experimentally deal with the effects of the high-frequency excitation on a buckled beam. Chelomei [6] shows from linear theoretical analysis that adding high-frequency axial excitation to the

This work was partially supported by the Japanese Ministry of Education, Culture, Sports, Science, and Technology, under Grants-in-Aid for Scientific Research 16560377.

H. Yabuno (✉) · K. Tsumoto
Graduate School of Systems and Information Engineering, University of Tsukuba, Tsukuba, Japan
E-mail: yabuno@esys.tsukuba.ac.jp
Tel.: +81-29-8536473
Fax: +82-29-8536471
E-mail: tsumoto@aosuna.esys.tsukuba.ac.jp
Tel.: +81-29-8536464
Fax: +82-29-8536471

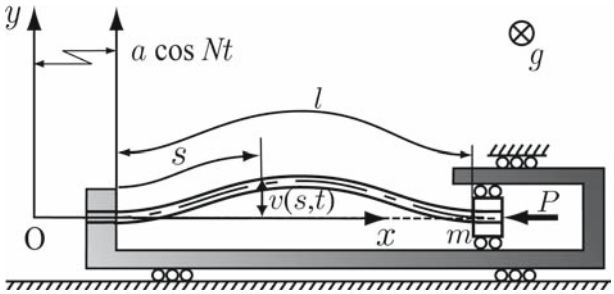

Fig. 1 Elastic beam subjected to an axial static force and high-frequency axial excitation

entirety of the beam can stabilize the simply supported buckled beam. The results are limited in the neighborhood of the straight position. On the other hand, Jensen [7] theoretically discusses nonlinear characteristics of the bifurcation of a compressive simply supported beam in the case when the high-frequency excitation is embedded in the compressive force. Also, for the same system and a cantilever beam, the stiffening effects of the high-frequency excitation are experimentally investigated [8,9]. In these studies, the nonlinear phenomenon which can be predicted from nonlinear theory is not experimentally confirmed. In this paper, the nonlinear dynamics of a clamped–clamped beam is experimentally investigated when the entirety of the beam is excited with high-frequency. The transient state from the buckled position to the straight position is experimentally observed under the high-frequency excitation. The bifurcation diagram is detected and the nonlinear characteristics are compared with one in the case without excitation.

2 Analytical model and buckling force

2.1 Equation of motion

We consider a clamped–clamped beam subjected to compressive force P as shown in Fig. 1. When the compressive force is over a critical value P_{cr}, the buckling occurs in the beam. In this study, we examine the nonlinear dynamics of the buckled beam in the case when the entirety of the system is excited with $x_e = a\cos Nt$; a is excitation amplitude and N is excitation frequency. The notation employed in this analysis is as follows: t is the time; s is the distance along not deformed neutral axis; x and y are the inertial coordinates; $v(s,t)$ are the displacement at the position s along the inertial axes y; and other parameters are as follows:

l: Length of the beam, m: end mass, ρA: line density of the beam

E: Young's modulus, I: moment of inertia of cross-sectional area.

Using the Bernoulli–Euler beam theory and assuming the inextensible condition, we can express the linearized equation of motion and the associated boundary conditions for the beam as

$$\rho A\frac{\partial^2 v}{\partial t^2} + EI\frac{\partial^4 v}{\partial s^4} + P\frac{\partial^2 v}{\partial s^2} - \left[\{\rho A(l-s)+m\}\frac{\partial^2 v}{\partial s^2} - \rho A\frac{\partial v}{\partial s}\right]aN^2\cos Nt = 0 \tag{1}$$

$$v\big|_{s=0} = \frac{\partial v}{\partial s}\big|_{s=0} = v\big|_{s=l} = \frac{\partial v}{\partial s}\big|_{s=l} = 0. \tag{2}$$

The following nondimensionalization is suitably employed to render the equation nondimensional:

$$t^* = Nt,\quad s^* = \frac{s}{l},\quad v^* = \frac{v}{l},\quad a^* = \frac{a}{l},\quad m^* = \frac{m}{\rho Al}\quad (18.23),$$

$$P^* = \frac{P}{\rho Al^2N^2}\quad (79.43P/N^2),\quad K^* = \frac{EI}{\rho Al^4N^2}\quad (12.42/N^2),$$

where the star indicates nondimensional variables; P^* is the dimensionless compressive force and K^* is the dimensionless flexural rigidity. The values for the subsequent experimental setup are also given in the

parenthesis. The dimensionless equation of motion and associated boundary conditions are

$$\ddot{v}^* + K^* v^{*\prime\prime\prime\prime} + P^* v^{*\prime\prime} - a^* \cos t^* \{(1 + m^* - s^*) v^{*\prime\prime} - v^{*\prime}\} = 0 \tag{3}$$

$$v^*\big|_{s^*=0} = v^{*\prime}\big|_{s^*=0} = v^*\big|_{s^*=1} = v^{*\prime}\big|_{s^*=1} = 0, \tag{4}$$

where [˙] and [′] are replaced by $\partial/\partial t^*$ and $\partial/\partial s^*$, respectively. Hereafter, the star will be dropped for ease of notation and the employed variables will be nondimensional unless otherwise specified.

2.2 Buckling force of compressive beam

In this section, we consider the equation of the motion in which the excitation is neglected.

$$\ddot{v} + P v'' + K v'''' = 0 \tag{5}$$

$$v(0) = v'(0) = v(1) = v'(1) = 0. \tag{6}$$

Separating variables as

$$v = X(t)\phi(s) \tag{7}$$

and letting $\ddot{v} = 0$ leads to

$$K v'''' + P v'' = 0, \tag{8}$$

$$v(0) = v'(0) = v(1) = v'(1) = 0. \tag{9}$$

The smallest P satisfying Eqs. (8) and (9)is the buckling force for the first mode and is expressed as

$$P \equiv P_{\mathrm{cr}} = 4\pi^2 K. \tag{10}$$

Then, the mode shape can be expressed as

$$\Phi_1(s) = 1 - \cos\, 2\pi s. \tag{11}$$

3 Increase of the buckling force by added high-frequency excitation

3.1 Averaged equation

A third-order expansion of the solutions of the equation of motion is

$$v = \epsilon v_1(t_0, t_1, t_2) + \epsilon^2 v_2(t_0, t_1, t_2) + \epsilon^3 v_3(t_0, t_1, t_2), \tag{12}$$

where ϵ is a small parameter ($|\epsilon| \ll 1$) of a book-keeping device and the multiple time scales [10] are introduced as follows:

$$t_0 = t, \quad t_1 = \epsilon t, \quad t_2 = \epsilon^2 t. \tag{13}$$

We rewrite the compressive force P as

$$P = P_{\mathrm{cr}} + \Delta p, \tag{14}$$

where Δp is a detuning parameter which expresses the nearness of the compressive force P from the buckling force P_{cr}. Furthermore, we perform the scaling of some parameters according to

$$a = \epsilon \hat{a}, \quad \Delta p = \epsilon^2 \Delta \hat{p}, \tag{15}$$

where $\hat{}$ denotes the order of $O(1)$. Substituting Eqs. (12), (14), and (15) into Eqs. (3) and (4) yields the following equation of the orders $O(\epsilon)$, $O(\epsilon^2)$, and $O(\epsilon^2)$:

$$O(\epsilon) : D_0^2 v_1 + P_{\rm cr} v_1'' + K v_1'''' = 0 \tag{16}$$

$$O(\epsilon^2) : D_0^2 v_2 + P_{\rm cr} v_2'' + K v_2'''' = -2D_0 D_1 v_1 - \hat{a}\cos t_0\{(1+m-s){v_1}'' - {v_1}'\} \tag{17}$$

$$O(\epsilon^3) : D_0^2 v_3 + P_{\rm cr} v_3'' + K v_3'''' = -2D_0 D_1 v_2 - 2D_0 D_2 v_1 - D_1^2 v_1 - \Delta\hat{p} v_1'' + \hat{a}\cos t_0\{(1+m-s){v_2}'' - {v_2}'\}, \tag{18}$$

where $D_n = \partial/\partial t_n \quad (n = 0, 1, 2)$. The associated boundary conditions are

$$v_1(0) = v_1'(0) = v_1(1) = v_1'(1) = 0 \tag{19}$$

$$v_2(0) = v_2'(0) = v_2(1) = v_2'(1) = 0 \tag{20}$$

$$v_3(0) = v_3'(0) = v_3(1) = v_3'(1) = 0. \tag{21}$$

Using Eqs. (8) and (9), Eq. (16) leads to $D_0^2 v_1 = 0$. Therefore, the general solution of Eqs. (16) and (19) can be written as

$$v_1 = \{A_0(t_1, t_2)t_0 + A_1(t_1, t_2)\}\,\Phi_1(s). \tag{22}$$

We note that the first term is a secular term. For a uniform expansion, this term must be eliminated by setting A_0 to zero. Then, the general solution becomes

$$v_1 = A_1(t_1, t_2)\Phi_1(s). \tag{23}$$

Substituting Eq. (23) into Eq. (17), we have

$$D_0^2 v_2 + P_{\rm cr} v_2'' + K v_2'''' = \frac{\hat{a}}{2}\left[\{(1-s){\Phi_1}'' - {\Phi_1}'\} + m\Phi_1''\right]A_1(t_1, t_2)\mathrm{e}^{it_0} + c.c., \tag{24}$$

where c.c. denotes the complex conjugate of the preceding terms. Because no terms in the right hand side produce the secular term in the solution of v_2, a particular solution of v_2 can be written as follows:

$$v_2 = \hat{a}A_1(t_1, t_2)\mathrm{e}^{it_0}\Phi_2(s) + c.c. \tag{25}$$

Substituting Eq. (25) into Eq. (24) yields

$$\begin{aligned} K\Phi_2'''' + P_{\rm cr}\Phi_2'' - \Phi_2 &= \frac{1}{2}\{(1-s){\Phi_1}'' - {\Phi_1}'\} + \frac{1}{2}m\Phi_1'', \\ &= \frac{1}{2}\left(\beta^2\cos\beta s - \beta\sin\beta s - \beta^2 s\cos\beta s\right) + \frac{1}{2}m\beta^2\cos\beta s, \end{aligned} \tag{26}$$

where $\beta = 2\pi$ and the associated boundary conditions are

$$\Phi_2(0) = \Phi_2'(0) = \Phi_2(1) = \Phi_2'(1) = 0. \tag{27}$$

The general solution of Φ_2 is expressed as

$$\Phi_2 = \tilde{\Phi}_2 + \Phi_{2p}, \tag{28}$$

where $\tilde{\Phi}_2$ and Φ_{2p} are the homogeneous and a particular solution of Eqs. (26) and (27). Also, a particular solution Φ_{2p} is expressed as

$$\Phi_{2p} = f_1\cos\beta s + f_2\sin\beta s + f_3 s\cos\beta s, \tag{29}$$

where

$$f_1 = -\frac{1}{2}\beta^2(1+m), \quad f_2 = \frac{(2K-1)\beta^5 + \beta^3 + \beta}{2(\beta^4 - \beta^2 - 1)}, \quad f_3 = \frac{-\beta^2}{2(\beta^4 - \beta^2 - 1)}. \tag{30}$$

The homogeneous solution is

$$\tilde{\Phi}_2 = h_1\cos qs + h_2\sin qs + h_3\cosh ps + h_4\sinh ps, \tag{31}$$

where

$$p = \sqrt{\frac{-P_{\rm cr} + \sqrt{{P_{\rm cr}}^2 + 4K}}{2K}}, \quad q = \sqrt{\frac{P_{\rm cr} + \sqrt{{P_{\rm cr}}^2 + 4K}}{2K}}.$$

Substituting Eqs. (29) and (31) into Eq. (28) and taking into account the boundary conditions of Eq. (27) determine the coefficients of Eq. (31) as shown in Appendix A. Furthermore, substituting Eqs. (23) and (25) into Eq. (18), we have

$$\begin{aligned} D_0^2 v_3 + P_{\rm cr} v_3'' + K v_3'''' = &-\Phi_1 D_1^2 A_1 - {\Phi_1}'' \Delta\hat{p} A_1 + \hat{a}^2\{(1+m-s){\Phi_2}'' - {\Phi_2}'\}A_1 \\ &-2i\hat{a}\Phi_2 D_1 A_1(\mathrm{e}^{it_0} + \mathrm{e}^{-it_0}) \\ &+\frac{1}{2}\hat{a}^2\{(1+m-s){\Phi_2}'' - {\Phi_2}'\}(\mathrm{e}^{2it_0} + \mathrm{e}^{-2it_0}). \end{aligned} \tag{32}$$

The particular solution can be written in the form:

$$v_{3p} = \Phi_{3\_DC}(t_1, t_2, s) + \Phi_{3\_t_0}(s)A_1(t_1, t_2)\mathrm{e}^{it_0} + \Phi_{3\_2t_0}(s)A_1(t_1, t_2)\mathrm{e}^{2it_0} + c.c. \tag{33}$$

Because v_1 is independent of t_0 from Eq. (23), the first term of $\Phi_{3\_DC}(t_1, t_2, s)$ in the particular solution can be the secular term for v_3. The condition not to produce the secular term is equivalent to the solvability condition of Φ_{3_DC}. Substituting $v_{3p} = \Phi_{3\_DC}(t_1, t_2, s)$ into Eq. (32) yields

$$K\Phi_{3\_DC}'''' + P_{\rm cr}\Phi_{3\_DC}'' = -\Phi_1 D_1^2 A_1 - {\Phi_1}''\Delta\hat{p}A_1 + \hat{a}^2\{(1+m-s)\Phi_2'' - \Phi_2'\}A_1 \tag{34}$$

$$\Phi_{3\_DC}(0) = {\Phi_{3\_DC}}'(0) = \Phi_{3\_DC}(1) = {\Phi_{3\_DC}}'(1) = 0. \tag{35}$$

Multiplying Eq. (34) by Φ_1, integrating the result from s=0 to s=1, and taking into account the boundary conditions Eq. (35), the solvability condition of Eqs. (34) and (35) can be expressed as

$$D_1^2 A_1 + (C_1\Delta\hat{p} - C_2\hat{a}^2)A_1 = 0, \tag{36}$$

where

$$\begin{aligned} C_1 &= \int_0^1 \Phi_1{\Phi_1}''\mathrm{d}s \Big/ \int_0^1 {\Phi_1}^2\mathrm{d}s \quad (-13.16), \\ C_2 &= \int_0^1 \Phi_1\{(1+m-s){\Phi_2}'' - {\Phi_2}'\}\mathrm{d}s \Big/ \int_0^1 {\Phi_1}^2\mathrm{d}s \quad (-3.12\times10^4 \text{in the case of } N/2\pi = 33\,\mathrm{Hz}), \end{aligned} \tag{37}$$

where the values corresponding to the system in subsequent experimental setup are shown in the parenthesis. By multiplying ϵ^3 and taking into account Eqs. (15) and (36) leads to

$$\frac{\mathrm{d}^2 A}{\mathrm{d}t^2} + (C_1\Delta p - C_2 a^2)A = 0, \tag{38}$$

where $A = \epsilon A_1$ and $2A$ is the deflection at the midpoint of the beam. Then the approximate solution can be expressed as

$$v = \epsilon v_1 + O(\epsilon^2) = \epsilon A_1\Phi_1(s) + O(\epsilon^2) = A\Phi_1(s) + O(\epsilon^2), \tag{39}$$

where the time-variation of A is governed with Eq. (38).

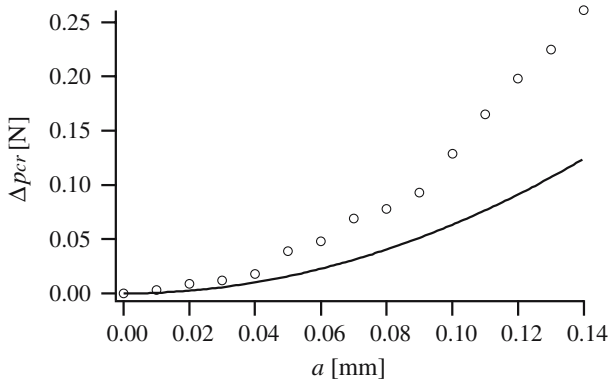

Fig. 2 Dependence of excitation amplitude on the buckling force ($N/2\pi = 33$ Hz)

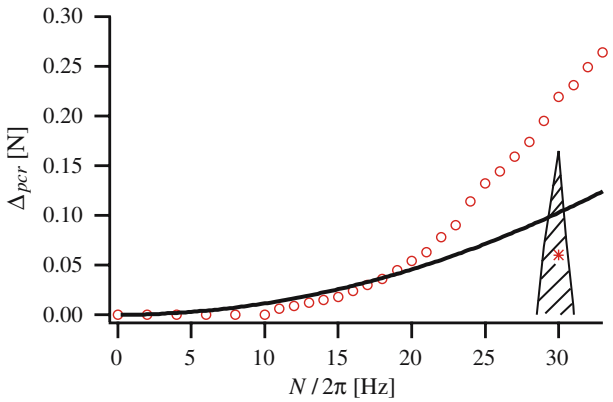

Fig. 3 Dependence of excitation frequency on the buckling force ($a = 0.14$ mm)

3.2 Linear analysis

The autonomous equation (38) enables us to perform the stability analysis of the trivial equilibrium point under the excitation. The sign of the coefficient of the second term in the left-hand side $k_{\text{equiv}} = C_1 \Delta p - C_2 a^2$, i.e. equivalent stiffness, determines the stability. When the sign is positive and negative, the trivial equilibrium point is stable and unstable, respectively. The critical point of the buckling corresponds to the case of $k_{\text{equiv}} = 0$. Of course in the case without excitation ($a = 0$), $\Delta p = 0$ satisfies $k_{\text{equiv}} = 0$. The dependence of Δp_{cr} on the excitation amplitude is shown in Fig. 2. The buckling force is increased with the excitation amplitude under constant excitation frequency $N/2\pi = 33$ Hz.

The critical point shifts from $p = p_{\text{cr}}$ to $p = p_{\text{cr}} + \Delta p_{\text{cr}}$ where $\Delta p_{\text{cr}} = c_2 a^2 / c_1$. The solid line in Fig. 3 shows the relationship between the shift of the critical point Δp_{cr} and the excitation frequency N under the constant excitation amplitude $a = 0.14$ mm; the circles show the experimental results mentioned later. It is theoretically predicted that the buckling force increases with the excitation frequency N.

4 Experiment

4.1 Experimental setup

We perform experiments to examine effects of high-frequency excitation on the buckled beam. We show the experimental apparatus in Figs. 4 and 5. The test specimen employed in the experimental investigations is a uniform with rectangular cross section made of phosphor bronze and it is rigidly clamped at the both end in the lateral direction (Fig. 6). We note that the width direction has been placed in a vertical plane to overcome the presence of the initial static curvature due to gravity. One of the supporting points is rigidly clamped on an aluminum slab. The other end is mounted on top of a sliding linear bearing (IKO Ball Slide Unit, Model

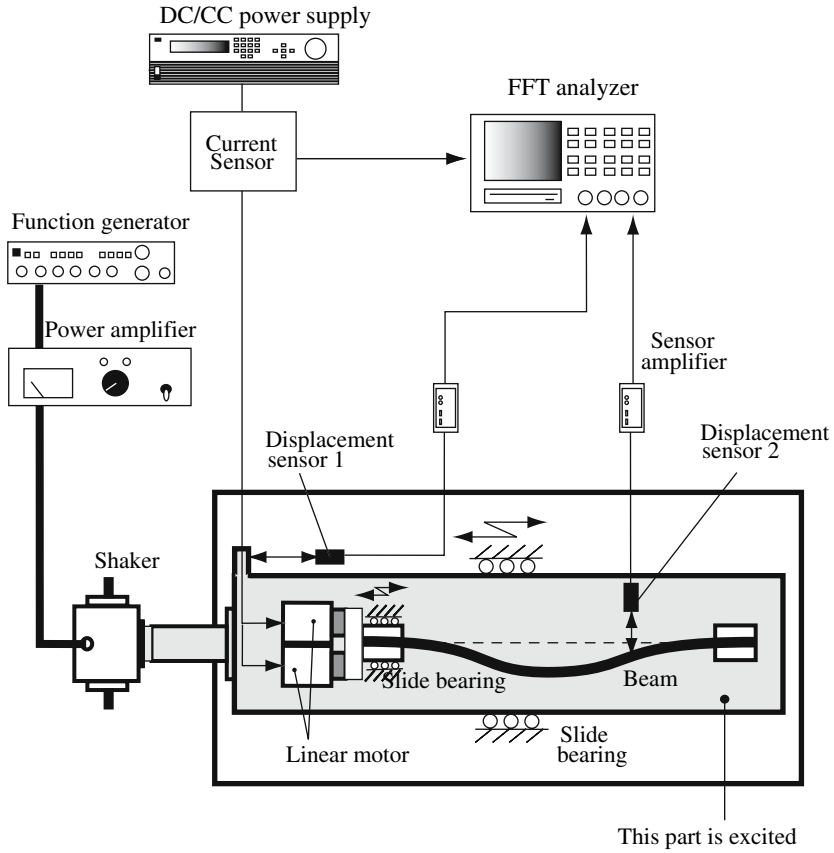

Fig. 4 Experimental apparatus

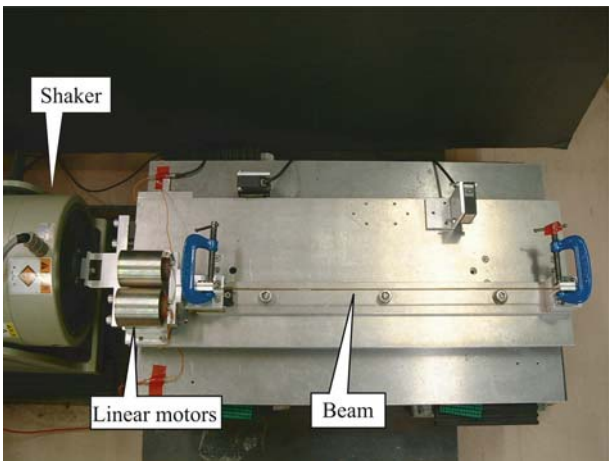

Fig. 5 Setup of the beam

BSU 44-50 A) with an end mass m; the first and second natural frequencies are 12.55 and 34.5 Hz, respectively. On the end of the linear bearing, two linear motors (Showa-Densen-Denran Model 26-02R) apply the static compressive force. Force of the motor is proportional to the input current to the motor. The current is produced by a power supply unit (KIKUSUI Corp., PBX40-10). Also, the excitation in the axial direction for the stabilization of the buckling is added by a shaker (EMIC 371-A). The excitation amplitude and frequency are adjusted by a function generator (TOA FS-2201). Laser displacement sensors, 1 and 2 (KEYENCE Corp.,

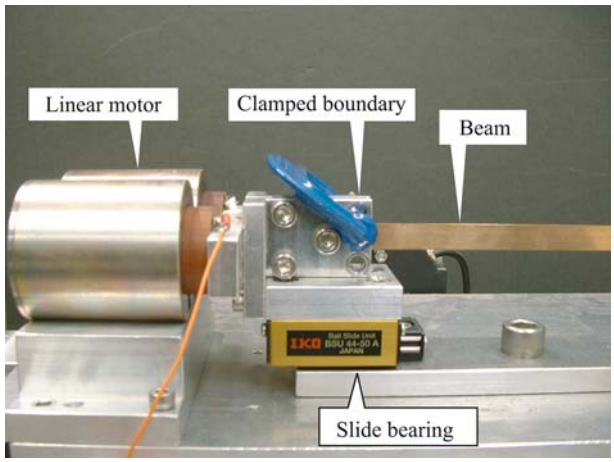

Fig. 6 Expanded view of the sliding end

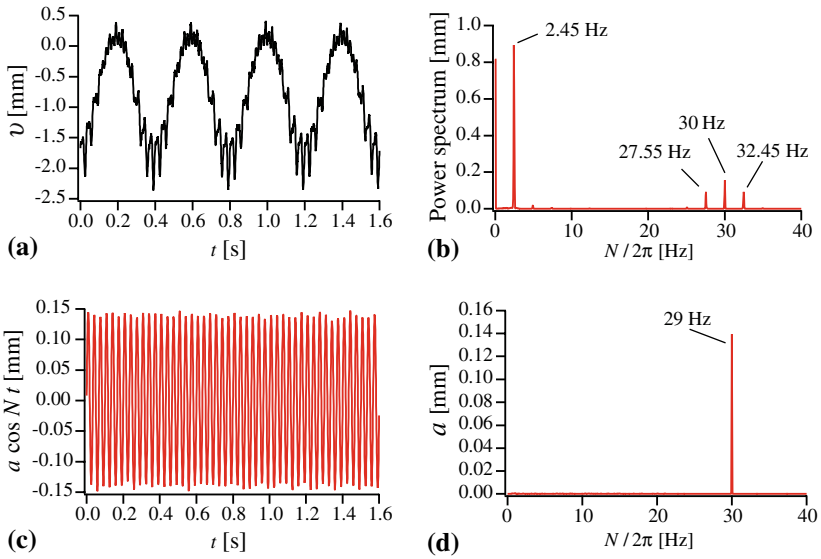

Fig. 7 Resonance of beam under high-frequency excitation ($N/2\pi = 30$ Hz, $a = 0.14$ mm, $\Delta p = 0.06$ N). **a** Time history of the beam. **b** Power spectrum of time history of beam. **c** Time history of the excitation. **d** Power spectrum of time history of excitation

LB-01) are used to measure the axial excitation and the displacement of the beam at one-quarter of the beam span from the fixed end. The main properties of the beam are summarized as follows:

$l = 4.50 \times 10^{-1}$ m, $m = 5.1 \times 10^{-1}$ kg, $\rho A = 6.21 \times 10^{-2}$ kg/m,
$E = 1.11 \times 10^{11}$ N/m^2, $I = 2.86 \times 10^{-13}$ m^4.

4.2 Experimental result and discussion

First, by quasi-stationary increasing the compressive force, the buckling force without excitation is measured and turned out to be $P_{\rm cr} = 5.925$ N, whereas theoretical prediction is 6.174 N.

We investigate change of the critical buckling force depending on the excitation amplitude under the constant excitation frequency (33 Hz). Figure 2 shows the relationship between the buckling force and the excitation amplitude. The buckling force is monotonically increased with the excitation amplitude. The experimental results qualitatively correspond well to the theoretical ones. Quantitative discrepancy may be due to the luck of consideration of extension and shear deformation in the theory.

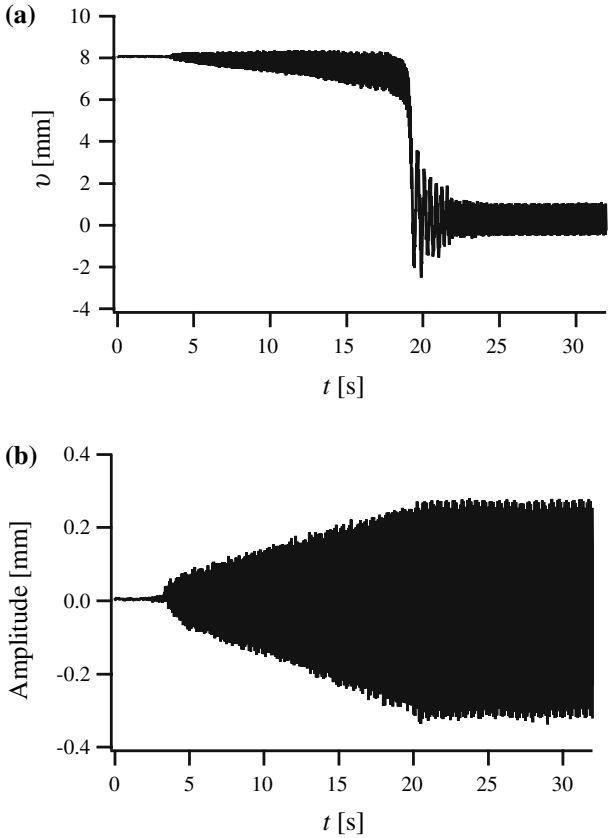

Fig. 8 Stabilization of buckled beam to the straight position ($N/2\pi = 18$ Hz, $P = 6.01$ N). **a** Time history of beam. **b** Time history of excitation

Next, we investigate the change of the buckling force depending on the excitation frequency under constant excitation amplitude (0.14 mm). Figure 3 shows the relationship between the excitation frequency N and the increase of the buckling force $\Delta p_{\rm cr}$. Experimental results indicate that the increase of the excitation frequency enlarges the buckling force as the theoretical result (solid line). In the hatched region of Fig. 3, certain resonances are observed. For example, at the condition of the symbol * in Fig. 3 ($N/2\pi = 30$ Hz, $a = 0.14$ mm, and $\Delta p = 0.06$ N), the beam is excited as shown in Fig. 7; the biggest frequency component of the beam is 2.45 Hz, though the excitation frequency is 30 Hz.

We set the compressive force $P = 6.01$ N which is larger than the buckling force. We examine the time history of the beam when the excitation amplitude is increased under constant excitation frequency ($N/2\pi = 18$ Hz). In this experiment, we manually increase the excitation amplitude with a constant excitation frequency $N/2\pi$ =18 Hz. Figure 8a, b show the time histories of the deflections of the beam and of the excitation in the axial direction, respectively. The beam is initially in the post buckling state. At $t = 3$ s, we start exciting the beam in the axial direction by the shaker and gradually increase the excitation amplitude until $a = 0.29$ mm. When the excitation amplitude becomes 0.27 mm, the transient state of the beam starts for recovering to the straight position. Finally, the buckled beam is stabilized in the neighborhood of the trivial equilibrium point which is unstable in the case without excitation.

Next, we show experimentally obtained bifurcation diagrams in the cases without and with excitation in Figs. 9a, b, respectively. The circle denotes stable equilibrium point. Because of initial imperfection of the beam, the experimentally obtained diagram in Fig. 9a shows a perturbed supercritical pitchfork bifurcation. Comparing the stable trivial equilibrium points of Figs. 9a, b, we can experimentally confirm that the buckling force is increased as the results of linear analysis. Furthermore, the supercritical pitchfork bifurcation in the case without excitation is not simply shifted in the right direction by the excitation. In the region below the increased buckling force in Fig. 9b, two stable nontrivial equilibrium states coexist with the trivial stable equilibrium state. This phenomenon corresponds to the nonlinear feature [7], which is theoretically predicted

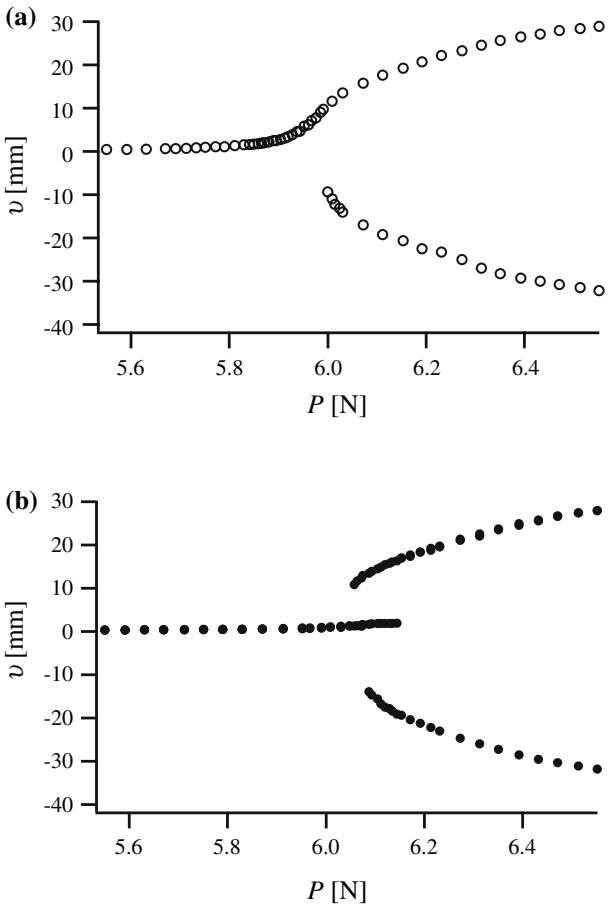

Fig. 9 Relationship between deflection of the beam v and axial compressive force P. **a** Without excitation. **b** With excitation ($N/2\pi = 33$ Hz, $a = 0.14$ mm)

by using a little different system from the present system. It appears that the bifurcation point at the increased buckling force is not supercritical but subcritical pitchfork bifurcation coexisting with two saddle-node bifurcations. In order to detect the nonlinear feature of the beam under high-frequency excitation, extensibility and shearability should be taken into account.

Figure 9b consists of data obtained by some quasi-stationary sweeps of P. On the other hand, the bullet• of Fig. 10a–c and shows separately equilibrium points obtained by each quasi-stationary sweep. For reference every figure in Fig. 10, the stable equilibrium points in the case without excitation are shown by ∘. Figure 10a represents the equilibrium points in the quasi-stationary forward sweep of P. Figure 10b represents the equilibrium points in the quasi-stationary backward sweep of P from an upper stable nontrivial equilibrium point. Figure 10c represents the equilibrium points in the quasi-stationary backward sweep of P from a lower stable nontrivial equilibrium point.

5 Conclusion

In this research, we experimentally investigate the influence of high-frequency excitation on the nonlinear dynamics of a bucked beam. First, we apply linear theory to the analytical model neglecting the nonlinearity, extensibility, and shearability. It is theoretically shown that the buckling force is enlarged as the excitation amplitude or frequency increases. The same feature is experimentally confirmed, though there are discrepancies with the theoretical results. Theoretical approach by considering extensibility and shearability may produce quantitative good agreement with experimental results. In a range of excitation condition, high-frequency excitation induces resonance with much lower frequency component than excitation frequency. The bifurcation diagram is experimentally obtained, and it is experimentally clarified that the high-frequency excitation does

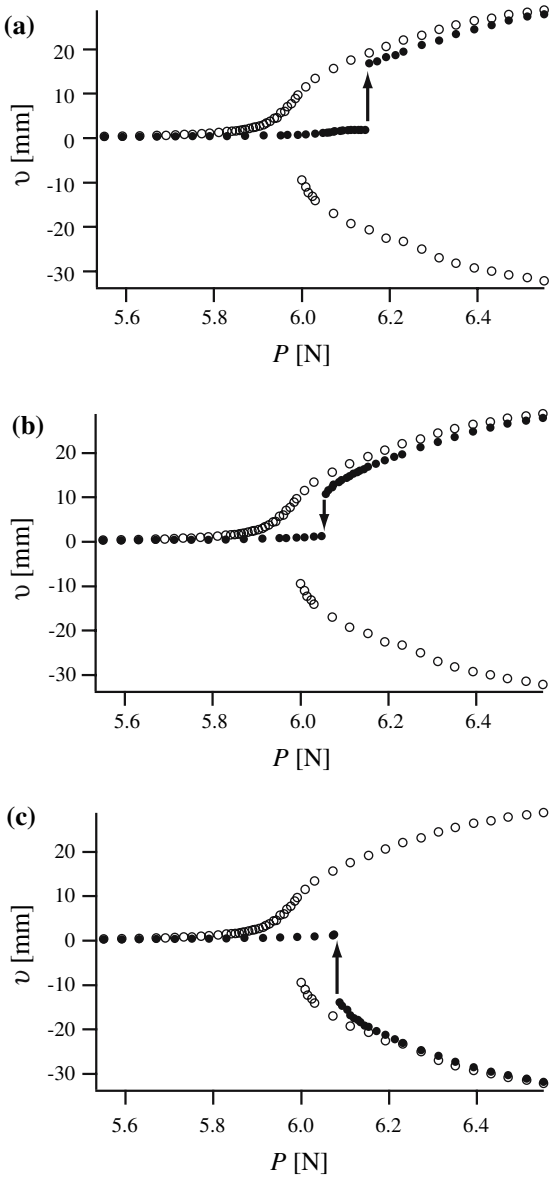

Fig. 10 Stable equilibrium points under quasi-stationary sweep of P. **a** Forward sweep of P. **b** Backward sweep of P (initial condition of v is the *upper right end point*). **c** Backward sweep of P (initial condition of v is the *lower right end point*)

not simply shift the bifurcation point of the buckling, but changes the nonlinear characteristics from supercritical to subcritical. As a result, the stable steady state of the beam exhibits hysteresis as the compressive force is reversed. From the above mentioned discrepancy between the theoretical and experimental results and the experimentally obtained bifurcation diagram, it appears that the effects of extensibility and shearability together with nonlinear curvature should be taken into account to theoretically investigate nonlinear dynamics of buckled beam under high-frequency excitation. The nonlinear formulation of governing equations and nonlinear analysis are in future work.

Acknowledgements First, the authors wish to thank Professor J. Awrejcewicz (Department of Automatics and Biomechanics, Technical University of Lodz) who gives a very valuable opportunity of plenary lecture at 8th Conference on Dynamical Systems Theory and Applications. And also, the first author wishes to thank Professor J.J. Thomsen (Department of Solid Mechanics, Technical University of Denmark) who gives a very impressive presentation on interesting phenomena under high-frequency excitation at ICTAM 2000.

Appendix A

$$
\begin{aligned}
h_1 = 2\pi^2\Big[&-p\cosh\ p[q\{4\pi^2(-1+4\pi^2)+m(-1-4\pi^2+16\pi^4)\}\\
&+q\cos\ q(1+m)(-1-4\pi^2+16\pi^4)-2\sin\ q\{1+2\pi^2+8\pi^4(-1+2K)\}]\\
&+p\Big[q(1+m)(-1-4\pi^2+16\pi^4)+q\cos\ q\{4\pi^2(-1+4\pi^2)+m(-1-4\pi^2+16\pi^4)\}\\
&-\sin\ q\{1+2\pi^2+8\pi^4(-1+2K)\}-\sinh\ p[-2q\{1+2\pi^2+8\pi^4(-1+2K)\}\\
&+2q\cos\ q\{1+2\pi^2+8\pi^4(-1+2K)\}-p^2\sin\ q(1+m)(-1-4\pi^2+16\pi^4)]\Big]\Big]\\
&\Big/[(-1-4\pi^2+16\pi^4)\{2pq-2pq\cos\ q\cosh\ p+\sin\ q\sinh\ p(p^2-q^2)\}]
\end{aligned}
\tag{40}
$$

$$
\begin{aligned}
h_2 = -2\pi^2\Big[&p\cosh\ p[2+4\pi^2-16\pi^4+32K\pi^4+2\cos\ q\{1+2\pi^2+8(-1+2K)\pi^4\}\\
&+q\sin\ q(1+m)(-1-4\pi^2+16\pi^4)]-p\Big[[2+4\pi^2-16\pi^4+32K\pi^4\\
&+2q\sin\ q\cos\ q\{1+2\pi^2+8(-1+2K)\pi^4\}(-m-4\pi^2-4m\pi^2+16\pi^4+16m\pi^4)]\\
&+\sinh\ p[p^2(m+4\pi^2+4m\pi^2-16\pi^4-16m\pi^4)+p^2\cos\ q(1+m)(-1-4\pi^2+16\pi^4)\\
&+2\{1+2\pi^2+8\pi^4(-1+2K)\}]\Big]\Big]\\
&\Big/[(-1-4\pi^2+16\pi^4)\{2pq-2pq\cos\ q\cosh\ p+\sin\ q\sinh\ p(p^2-q^2)\}]
\end{aligned}
\tag{41}
$$

$$
\begin{aligned}
h_3 = -2\pi^2\Big[&p[-q(1+m)(-1-4\pi^2+16\pi^4)+q\cos\ q\{4\pi^2(-1+4\pi^2)\\
&+m(-1-4\pi^2+16\pi^4)\}-2\sin\ q\{1+2\pi^2+8\pi^4(-1+2K)\}]\\
&+p\cosh\ p[q(m+4\pi^2+4m\pi^2-16\pi^4-16m\pi^4)+q\cos\ q(1+m)(-1-4\pi^2+16\pi^4)\\
&+2\sin\ q\{1+2\pi^2+8\pi^4(-1+2K)\}]+q\sinh\ p[2+4\pi^2-16\pi^4+32K\pi^4\\
&-2\cos\ q\{1+2\pi^2+8\pi^4(-1+2K)\}+q\sin\ q(1+m)(-1-4\pi^2+16\pi^4)]\Big]\\
&\Big/[(-1-4\pi^2+16\pi^4)\{2pq-2pq\cos\ q\cosh\ p+\sin\ q\sinh\ p(p^2-q^2)\}]
\end{aligned}
\tag{42}
$$

$$
\begin{aligned}
h_4 = 2\pi^2\Big[&q\cosh\ p[2+4\pi^2-16\pi^4+32K\pi^4-2\cos\ q\{1+2\pi^2+8\pi^4(-1+2K)\}\\
&+q\sin\ q(1+m)(-1-4\pi^2+16\pi^4)]+q[2+4\pi^2-16\pi^4+32K\pi^4\\
&-2\cos\ q\{1+2\pi^2+8\pi^4(-1+2K)\}-q\sin\ q(-m-4\pi^2-4m\pi^2+16\pi^4+16m\pi^4)]\\
&+p\sinh\ p[q(m+4\pi^2+4m\pi^2-16\pi^4-16m\pi^4)+q\cos\ q(1+m)(-1-4\pi^2+16\pi^4)\\
&+2\sin\ q\{1+2\pi^2+8\pi^4(-1+2K)\}]\Big]\\
&\Big/[(-1-4\pi^2+16\pi^4)\{2pq-2pq\cos\ q\cosh\ p+\sin\ q\sinh\ p(p^2-q^2)\}]
\end{aligned}
\tag{43}
$$

References

1. Thomsen, J.J.: Slow high-frequency effects in mechanics: problems, solutions, potentials. In: Proceedings of ENOC-2005, Eindhoven, August 7–12, pp. 143–193 (2005)
2. Blekhman, I.I.: Vibrational Mechanics. World Scientific, Singapore (2000)
3. Stephenson, A.: On a new type of dynamical stability. In: Memoirs and Proceedings of the Manchester Literary and Philosophical Society, vol. 52, pp. 1–10 (1908)
4. Kapitza, P.L.: Collected Papers by P.L. Kapitza, vol. 2, pp. 714–726. Pergamon Press, London (1965)
5. Yabuno, H., Matsuda, T., Aoshima, N.: Reachable and stabilizable area of an underactuated manipulator without state feedback control. IEEE/ASME Trans. Mechatron. **10**, 397–403 (2005)
6. Chelomei, V.N.: On the possibility of increasing the stability of elastic systems by using vibration (in Russian). Doklady Akademii Nauk SSSR **110**(3), 345–347 (1956)
7. Jensen, J.S.: Buckling of an elastic beam with added high-frequency excitation. Int. J. Nonlin. Mech. **35**(2), 217–227 (2000)

8. Jensen, J.S., Tcherniak, D.M., Thomsen, J.J.: Stiffening effects of high-frequency excitation: experiments for an axially loaded beam. J. Appl. Mech. **67**, 397–402 (1999)
9. Thomsen, J.J.: Theories and experiments on the stiffening effect of high-frequency excitation for continuous elastic systems. J. Sound Vib. **260**, 117–139 (2002)
10. Nayfeh, A.H., Mook, D.T.: Nonlinear Oscillations. Wiley, New York (1979)